 doi:10.20944/preprints202108.0069.v1

Nanosensors based on structural memory carbon nanodots for Ag^+ fluorescence determination

Xi Zhou [123], Yufeng Cao [1], Xinji Zhou [1],Lina Xu [23], Daihui Zhang [23], Chunpeng Wang [23], Fuxiang Chu [23,*] , Tao Qian [1,*]

1 School of Chemistry and Chemical Engineering, Nantong University, Nantong 226019, China
2 Institute of Chemical Industry of Forestry Products, Chinese Academy of Forestry, Nanjing 210042, China
3 Co-Innovation Center of Efficient Processing and Utilization of Forest Resources, Nanjing Forestry University, Nanjing 210037, China

* Correspondence and requests for materials should be addressed to qiantao@ntu.edu.com (Tao Qian) or chufxg@163.com (Fuxiang Chu)

Abstract: Ag^+ pollution is great of harm to the human body and the biology. Therefore, it is an urgent need to develop inexpensive and accurate detection methods. Herein, lignin-derived structural memory carbon nanodots (C_{SM}-dots) with outstanding fluorescence property were fabricated via a green method, which reserve functional and structural units of the precursor molecules. The C_{SM}-dots could specifically bind Ag^+, accompanied with a remarkable fluorescence quenching response. This "turn-off" fluorescence behavior was used for Ag^+ determination in a linear range of 5-290 μM with the detection limit as low as 500 nM. Furthermore, the finding showed that this sensing nano-platform was successfully used for Ag^+ determination in real samples and intracellular imaging, showing great potential in biological and environmental monitoring applications.

Keywords: Carbon nanodots; Silver ion; Fluorescent sensor; Structural memory; Intracellular imaging

1. Introduction

In industrialized community, silver is one of the key ingredients in the field of pharmacy, photography, electrical and aerospace industry due to its attractive properties [1-3]. Ag^+ pollution has become a severe worldwide environmental problem with their potential harm to the human body and the biology [4]. Thus, it is great important to detect Ag^+ in water for living and production needs and various analytical strategies have been developed for quantitative determination of Ag^+, including atomic absorption spectrometry (AAS) [5], inductively coupled plasma optical emission spectrometer (ICP-OES) [6], inductively coupled plasma mass spectrometry (ICP-MS) [7] and electrochemical method [8]. However, these approaches suffer from either the expensive devices or the tedious sample pre-treatment process, which restrict their application in the field of fast monitor Ag^+. Therefore, the technique for rapid and effective detection towards Ag^+ is urgently demanded.

Over the past decades, optical sensors have been developed and utilized for Ag^+ determination at different levels [9-11]. Among them, fluorescent sensors are regarded as a powerful analytical strategy for Ag^+ detecting due to its inherent merits including easy operability, spatiotemporal resolution and high sensitivity and selectivity [12-15]. So far, series of fluorescent molecules have been prepared for Ag^+ analysis based on Ag^+-participated chelation or other chemical reactions [16-18]. While most reported fluorescent probes generally involve in complex preparation process with biotoxicity and low photostability. And the Ag^+ recognition reactions are susceptible to responsive environment, which severely limit its application [19-23]. Thus, further exploitation of eco-friendly Ag^+ sensors with nontoxicity and excellent photostability is still an important challenge for researchers.

Carbon nanodots (C-dots), as one of new members of carbon materials, have drawn impressive attention in the area of bio-labeling, cell-imaging, drug-delivery and so on [24-26]. Furthermore, it also can be used as a versatile platform for fluorescence (FL) sensing because of its unique photostability and FL emission, excellent water solubility, low toxicity and biocompatibility [27-30]. So far, various methods have been applied to preparing C-dots, such as electrochemical oxidation, microwave irradiation, arcdischarge and hydrothermal carbonization. The carbonization process of C-dots has always been triggered by

 doi:10.20944/preprints202108.0069.v1

microwave irradiation, acid treatment, electrochemical or heating techniques to structure conjugated carbon cores. Therefore, seeking for more ecofriendly and mild fabrication technologies for C-dots has received wide attention. What`s more, most sensing modes of C-dots depend on specific recognition groups or elements units obtained by surface chemical modification reaction, which can bind the target molecule resulting in FL changes of the C-dots [31-33]. However, another detection tactic based on "structural memory" of C-dots precursors is rarely reported. In general, the mild preparation conditions, particularly low pressure and temperatures, can make C-dots reserve functional and structural units of the precursor molecules without chemical reaction [34]. This detection strategy making full use of the specific recognition functional groups or atoms of the precursors to test target analytes is desirable.

Inspired by this, a novel sensor towards Ag^+ was developed based on structural memory C-dots (C_{SM}-dots), which were prepared by a facile and green strategy from sodium lignosulphonate under a mild preparation process. It is well known that lignin is one of main components in biomass and the aromatic structure with polyfunctional groups, which makes it suitable for green applications. In addition, the large number of hydroxyl, carboxyl, sulfonic acid group and other functional groups in the molecular structure of lignin has a good ability to capture the silver ions. In detail, as illustrating in Scheme 1, lignin was dissolved in polar solvent and formed nanodots in a low pressure and temperatures condition via a simple self-assembly method. After demonstration superior FL performance of lignin-derived nanodots, an eco-friendly Ag^+ sensor was prepared based on the aggregation induced quenching effect between Ag^+ and aromatic ring system of nanodots. Furthermore, this sensing platform was successfully applied for Ag^+ monitoring in real samples and intracellular imaging without surface chemical modification.

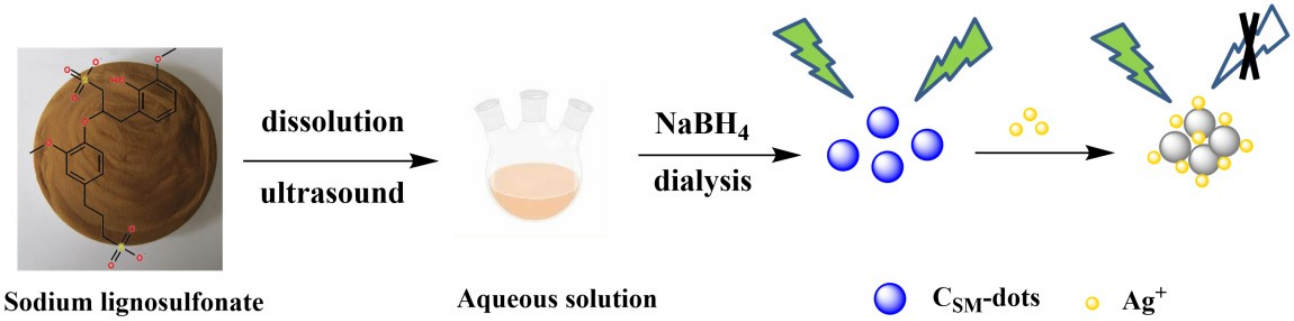

Scheme 1 Fabrication process of lignin-derived C_{SM}-dots

2. Materials & Methods

2.1 Materials

A variety of metal salts including $AgNO_3$, $Ni(NO_3)_2$, $BaCl_2$, $ZnCl_2$, $CuCl_2$, $CaCl_2$, KOH, NaCl, $AlCl_3$, $FeCl_2$, $MgCl_2$, $FeCl_3$, $MnCl_2$, $PbCl_2$, $Co(NO_3)_2$ and $NaBH_4$ were purchased from Nanjing Chemical Reagent Co., Ltd. (Nanjing, China). Sodium lignosulphonate was obtained from Macklin Biochemical Technology Co., Ltd. (Shanghai, China). All the chemicals were analytical grade and used without further purification. All aqueous solutions were made using deionized water.

2.2 Characterization

The transmission electron microscopic (TEM) images were acquired by JEM-2100 transmission electron microscopy (JEOL, Japan) at an accelerating voltage of 200 kV. The UV-vis spectra were recorded on UV-vis absorption spectrophotometer (UV-1800pc) at 800-200 nm. The X-ray photoelectron spectra (XPS) were measured by PHI 500 VersaProbe X-ray photoelectron spectrometer (UlVAC-PHI, Japan). The FT-IR spectra were obtained on iS10 FT-IR spectrometer at 500-5000 cm^{-1} (Nicolet, USA). Zeta potential was recorded on Zetasizer Nano ZS instrument (Malvern, U.K.). The FL spectra were acquired by LS SS Perkin Elmer spectrometer (Perkin Elmer, USA) with the slit widths of 4 nm for emission and excitation spectra. All the fluorescence spectra were measured from 330 nm to 700 nm with a quartz cuvette of 1 cm path length.

Preprints (www.preprints.org) | NOT PEER-REVIEWED | Posted: 3 August 2021 doi:10.20944/preprints202108.0069.v1

2.3 Preparation of lignin-derived C_{SM}-dots

In a typical procedure, sodium lignosulfonate (0.03 g) was dissolved into 15 mL deionized water completely. And the solution was treated by ultrasound for 90 min followed with stirring under 1 h. After that, the obtained solution was centrifuged for 30 min to remove precipitates. The supernatant was collected and mixed with $NaBH_4$ (0.5 mol/mL) to allow the formation of particles, and then further dialyzed using dialysis bag (1000 Da cut off) for 12 h. The C_{SM}-dots powder was acquired by freeze-drying for further use.

2.4 Fluorescence detection of Ag^+

A dispersion of the C_{SM}-dots was prepared in PBS buffer solution (0.1 M, pH 7.0) with a concentration of 0.05 mg/mL. 300 μL of C_{SM}-dots dispersion, 1200 μL of Ag^+ solution with different concentration (0–500 μM) and 1500 μL of ultrapure water were mixed in a quartz cuvette. And then, the mixture was moved for FL measurement at 325 nm excitation wavelengths after being incubated for 5 minutes at room temperature. The same method was applied for selectivity test, 1200 μL of aqueous solutions containing specific ion (400 μM) were introduced to above mixture for substituting Ag^+ solution.

3. Results

3.1 Physiochemical characterization of C_{SM}-dots

During the low temperature preparation process of C_{SM}-dots, a considerable portion of functional groups that belong to lignin were retained, which was confirmed by FT-IR (Fig. 1a). The peaks at 1704 and 1196 cm^{-1} resulted from the stretching vibration of conjugated C=O bonds and S=O bonds in sulfonic acid groups, respectively. The peaks at 1592 and 1043 cm^{-1} were attributed to the stretching vibrations of C=C bond in the aromatic skeleton and the deformation vibration of C−O−C groups, respectively. The presence of O−H groups was confirmed by the peaks around 3000-3500 cm^{-1} [25]. And the peak intensity in C_{SM}-dots increased, indicating that the addition of $NaBH_4$ produced more hydroxyl groups. More convincing detail on chemical composition of C_{SM}-dots was provided by the XPS spectrum (Fig. 1b). It was found in the full range XPS spectrum that three peaks at 168.08 eV, 285.08 eV and 533.08 eV were due to S 2p, C 1s and O 1s, respectively. Moreover, the high-resolution spectra showed further information on different types of chemical bonds. The C 1s spectrum (Fig. 1c) indicated the presence of C=C/C–C (284.7 eV), C=O (286.4 eV) and C-O/C-S (285.8 eV). The existence of C=C and C=O/C–O peaks further identifies that the C_{SM}-dots are enriched with carbonyl and carboxyl functional groups on the surface. The deconvoluted S 2p XPS spectrum (Fig. 1d) displayed four peaks at 161.2 eV (S $2p_{3/2}$), 162.4 eV (S $2p_{1/2}$), 168.3 eV (S-O_3) and 168.8 eV (S-O_4) binding energy, respectively, which clearly indicates that S atoms are present in the skeleton of C_{SM}-dots. And the spectrum of O 1s (Fig. S1a) can be divided into three peaks at 529.5, 531.1, and 533.2 eV, which corresponded to C=O/S=O, C−O/C−O−C, and Ar−OH bonds, respectively [37]. In addition, morphology and size distribution of the prepared C_{SM}-dots were showed in TEM image (Fig. S1b). The C_{SM}-dots were well dispersed with a narrow range of 8.2 to 23.5 nm. And almost 72% of the C_{SM}-dots were focus on an average diameter between 14.5 and 20.0 nm (Fig. S1c). The self-assembly of lignin was largely due to π-π interactions and inter/intramolecular hydrogen bonding [38]. A broad peak at 21.3° in the XRD patterns of C_{SM}-dots suggests an amorphous structure (Fig. S1d), which was due to the single benzene units and the weak interaction between themselves [39].

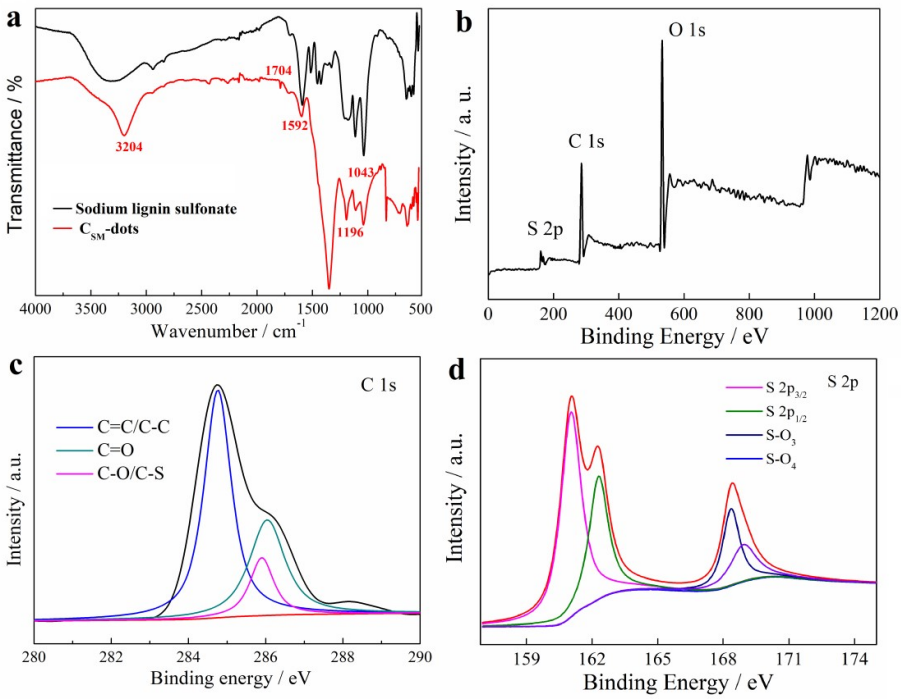

Fig. 1 (a) FT-IR spectra of lignin and C_{SM}-dots. (b) XPS spectrum of C_{SM}-dots. The high-resolution XPS spectra of C 1s (c) and S 2p (d) in C_{SM}-dots.

3.2 Optical properties of C_{SM}-dots

Optical performance of the C_{SM}-dots was characterized by the UV−vis absorption spectrum and the FL spectrum under different excitation wavelengths. Fig. 2a showed two obvious absorption peaks at 245 and 273 nm in UV−vis spectrum, which was ascribed to the typical absorptions of the π-π* transition and n-π* transition, respectively [9]. Above results are similar to that of multiple aromatic chromophores originated from lignin, suggesting the existence of aromatic structures in C_{SM}-dots [25]. The FL spectra showed that a maximum emission peak at 415 nm was obtained which resulted by monitoring the excitation from incident light at 325 nm. Additionally, the C_{SM}-dots exhibited an excitation-dependent FL behavior in an excitation wavelengths range of 240–440 nm (Fig. 2b). And the FL quantum yield of C_{SM}-dots in the aqueous solution was 13.3% (quinine sulfate as the standard), which is greater than the C-dots derived from biomass-based raw materials without doping [27]. The pH effects on FL intensity of the C_{SM}-dots were investigated (Fig. S2). It showed a pH-dependence on the FL intensity of the C_{SM}-dots, which might be due to pH-sensitive π−π interactions and hydrogen bonding, leading to weakening or strengthening in the FL emission intensity or wavelength. This result provides an evidence for the existence of π−π interactions-induced self-assembly in C_{SM}-dots. The effects of environment temperature and ionic strength on the FL property were also researched to test the FL stability of as-prepared C_{SM}-dots (Fig. S3a and S3b). The FL intensity of the C_{SM}-dots showed negligible changes under different temperature and ionic strengths conditions, suggesting that it can be used in different environments.

Preprints (www.preprints.org) | NOT PEER-REVIEWED | Posted: 3 August 2021 doi:10.20944/preprints202108.0069.v1

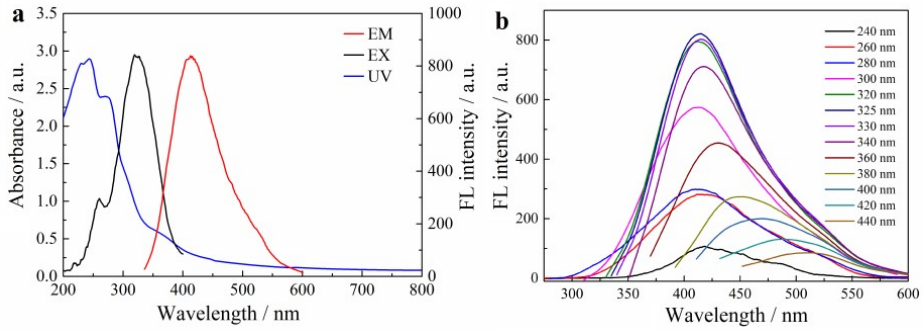

Fig. 2 (a) The UV-vis absorption spectra, FL excitation and emission spectra of C_{SM}-dots. (b) The FL emission spectra of C_{SM}-dots under different excitation wavelengths.

3.3 FL responses of C_{SM}-dots towards Ag^+ ions

Earlier reports have confirmed the strong interaction between Ag^+ and lignin based on its multiple aromatic functional groups in lignin [40]. Herein, the lignin-derived C_{SM}-dots reserving functional and structural units of the lignin molecules are expected to be a FL chemosensor towards Ag^+ due to the multiple recognition sites endowed by sodium lignosulfonate. The FL responses of C_{SM}-dots towards Ag^+ were demonstrated in Fig. 3a. It is found that the FL intensity of the C_{SM}-dots at 415 nm decreased with increasing the concentrations of Ag^+. And the relationships between the FL intensity and Ag^+ concentration are described by the Stern–Volmer equation [27]:

$$F_0/F = 1 + K_{SV}C_{Ag+}$$

where F_0 and F are the FL intensities in the absence and presence of Ag^+, respectively, K_{SV} is the quenching constant of Ag^+, and C_{Ag+} is Ag^+ concentration. As shown in the inset of Fig. 3a, an admirable linear FL response of C_{SM}-dots can be detected towards Ag^+, which was in a concentration range of 5-290 μM. A high linear correlation coefficient (R^2=0.994) was achieve with the limit of detection (LOD) as low as 500 nM (S/N=3). Moreover, the FL responses experiments towards other different ions (Ni^{2+}, Ba^{2+}, Zn^{2+}, Cu^{2+}, Ca^{2+}, K^+, Na^+, Al^{3+}, Fe^{2+}, Mg^{2+}, Fe^{3+}, Mn^{2+}, Pb^{2+}, Co^{2+}) were carried out under the same situation (Fig. 3b). And the addition of above potential interfering substances only brought about negligible changes in the FL intensity. The results of selectivity tests reflected the fact that the C_{SM}-dots had high selectivity for Ag^+ sensing, which provide the precondition for developing multi-functional sensing system.

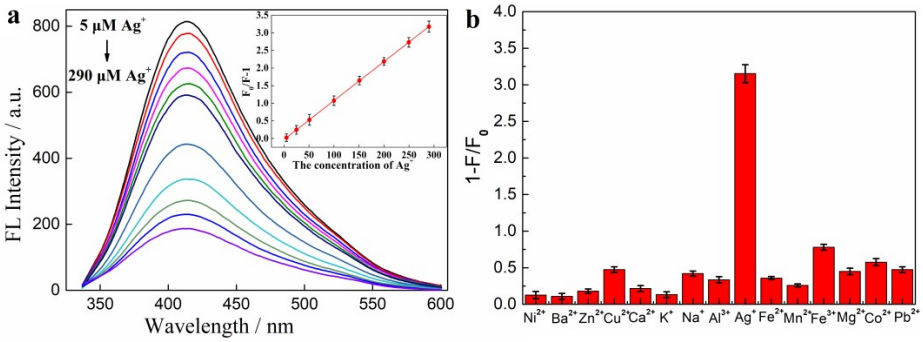

Fig. 3 (a) The FL emission spectra of C_{SM}-dots treated by different Ag^+ concentrations (from 5 to 290 μM). The inset is the relationship between the F_0/F value and Ag^+ concentrations. (b) FL responses of C_{SM}-dots in the presence of different metal ions. F_0 and F are the FL intensities in the absence and presence of metal ions, respectively.

A comparison of different methods for Ag^+ determination is summarized in Table S1, which shows the superiority of the proposed method in linear range and LOD. Furthermore, a static quenching process was obtained by the minor FL lifetime change (Fig. S4a). The average FL lifetime of C_{SM}-dots was transferred from 8.67 ns to 7.98 ns after the addition of Ag^+, which probably resulted from the formation of a quite stable nonradioactive FL complex between C_{SM}-dots and Ag^+ [37]. TEM coupled Zeta potential

Preprints (www.preprints.org) | NOT PEER-REVIEWED | Posted: 3 August 2021 doi:10.20944/preprints202108.0069.v1

characterization confirms the evidence of aggregation induced quenching mechanism. When 500 μM Ag^+ was added to the C_{SM}-dots solution with standing overnight, the TEM image displayed the obvious aggregation behavior (Fig. S4b). And the changes in zeta potential values of C_{SM}-dots from −8.32 to 3.37 mV after the addition of excess Ag^+, further suggests the aggregation effect between the lignin-derived C_{SM}-dots and Ag^+.

3.4 Cytotoxicity test

Biomass-derived C-dots have intrinsic biocompatibility and low toxicity, which provides advantaged conditions for its application in biological fields. Before biological application, the cytotoxicity experiments were carried out through MTT method, in which the viability of HeLa cells treated with C_{SM}-dots was evaluated. It was found in the cytotoxicity experiments that the viability of HeLa cell was shown to be more than 88% even at a concentration of 0.75 mg/mL, showing excellent biocompatibility and great promise for cellular imaging (Fig. 4).

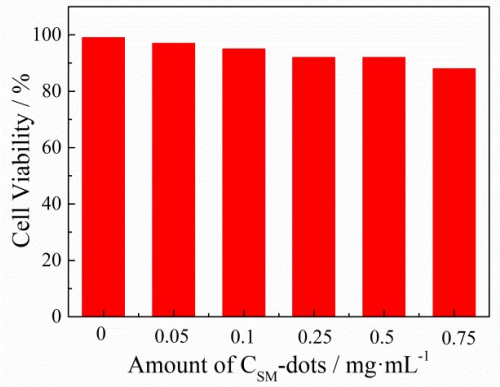

Fig. 4 HeLa cell viability after incubation with different concentrations of C_{SM}-dots for 24h

3.5 Practical assay in real sample and cellular imaging

To confirm the superiority of the approach in real sample, the C_{SM}-dots were employed to detect Ag^+ in tap water samples by standard addition method. Different concentration of Ag^+ was added into tap water samples in the presence of C_{SM}-dots. As shown in Table 1, recoveries between 90.7% and 106.3% with relative standard deviation (RSD) lower than 4.5% were achieved at each Ag^+ concentrations. These consequences suggest the reliability and feasibility of the C_{SM}-dots for Ag^+ monitoring in practical sample analysis. In addition, to further estimate the biologic applications of the C_{SM}-dots, cell imaging experiments were carried out to demonstrate their feasibility in biological applications. As shown in Fig. S5, an intracellular district displayed a remarkable blue emission. And there was no considerable alters in the morphology of HeLa cell, which proved the low cytotoxicity of the C_{SM}-dots. All results demonstrated that the prepared nanodots could be used for effectively labeling in live cells.

Table 1 Determination of Ag^+ in real samples.

Analyte	Spike (μM)	Found (μM)	Recovery (%)	RSD (n=3, %)
Ag^+	50.00	45.35	90.7	2.3
	100.00	96.4	96.4	3.7
	150.00	159.45	106.3	4.5
	250.00	263	105.2	4.4

4. Conclusions

In summary, a green, economical fabrication strategy for structural memory C_{SM}-dots was developed using sodium lignosulphonate as precursors. The as-prepared C_{SM}-dots with high FL performance were successfully utilized as sensing platform for Ag^+ determination. Due to the aggregation induced quenching effect of Ag^+ towards C_{SM}-dots and the high affinity between Ag^+, the proposed approach offers a rapid and

effective tactics for Ag^+ determination with excellent sensitivity and selectivity. More importantly, the designed sensor was successfully applied for Ag^+ monitor in real samples and cellular imaging, demonstrating the potential of the probe in practical applications. Therefore, we believed that this method might provide a new thought for exploitation multiple functional sensing platforms for the biological and environmental applications.

Supplementary Materials: Methodology of cytotoxicity test and cellular imaging analysis, Figure S1: (a) high-resolution XPS spectra of O 1s in C_{SM}-dots, (b) TEM image of C_{SM}-dots, (c) Size distribution of C_{SM}-dots, (d) XRD pattern of C_{SM}-dots, Figure S2: The effect of different pH value on the FL performance of C_{SM}-dots, Figure S3: FL intensity variation of the C_{SM}-dots as a function of temperature (a) and concentrations of NaCl (b), Table S1: Comparison of the reported probe for Ag^+ determination, Figure S4: (a) FL decay spectra of C_{SM}-dots and C_{SM}-dots/Ag^+ system, (b) The TEM image of C_{SM}-dots /Ag^+ composites, Figure S5: The fluorescence microscopy images of HeLa cells treated with C_{SM}-dots, (a) the bright-field images, (b) the fluorescent images, (c) the merged images of (a) and (b).

Author Contributions: Conceptualization, X.Z., F.X.C. and T.Q.; Methodology, X.Z., Y.F.C., X.J.Z., N.L.X. and D.H.Z.; Formal analysis, X.Z., Y.F.C., X.J.Z., N.L.X. and T.Q.; Funding acquisition, X.Z., C.P.W. F.X.C., and T.Q.; Investigation, Y.F.C., X.J.Z.; Project administration, X.Z., F.X.C. and T.Q.; data curation, X.Z., Y.F.C., X.J.Z., N.L.X. and D.H.Z.; Validation, C.P.W.; Writing—original draft, X.Z.; writing—review and editing, X.Z. All authors have read and agreed to the published version of the manuscript.

Funding: This work was funded by National Key Research and Development Program of China (No. 2017YFE0106800) and the National Natural Science Foundation of China (No. 32001284).

Conflicts of Interest: The authors declare no conflict of interest.

References

[1] Wang M, Zhang S, Du ZF, Sun LD, Zhao DL. Novel dye-sensitized solar cell architecture using TiO_2 coated Ag nanowires array as the photoanode. Rare Met. 2019; 38(4):316.

[2] Wu H, Kong DS, Ruan ZC, Hsu PC, Wang S, Yu ZF, Carney TJ, Hu LB, Fan SH, Cui Y. A transparent electrode based on a metal nanotrough network. Nat Nanotechnol. 2013; 8:421.

[3] Wang JC, Luo HS, Zhang MH, Zhu XH, Zhang J, Gu YX, Yi GB. Design and fabrication of a new fluorescence enhancement system of silver nanoparticles decorated aligned silver nanowires. Rare Met. 2019; 38(12):1178.

[4] Zhang F, Wu XL, Chen YY, Lin H. Application of silver nanoparticles to cotton fabric as an antibacterial textile finish. Fiber Polym. 2009; 10:496.

[5] Dadfarnia S, Haji Shabani AM, Gohari M. Trace enrichment and determination of silver by immobilized DDTC microcolumn and flow injection atomic absorption spectrometry. Talanta. 2004; 64:682.

[6] Yalcin MS. Solid phase extraction of trace level Ag(I) using coriolus versicolor immobilized magnetic nanoparticles and its determination by ICP-OES. Environ Prog Sustainable Energy. 2019; 38(4): e13251.

[7] Reddi GS, Rao CRM. Analytical techniques for the determination of precious metals in geological and related materials. Analyst. 1999; 124:1531.

[8] Hu Y, Zhuang XY, Lin LC, Liu JY, Yao ZY, Xiao ZY, Shi J, Fang BS, Hong WJ. Determination of Ag[I] and NADH using single-molecule conductance ratiometric probes. ACS Sens. 2021; 6(2):461.

[9] Wang ZH, Zhang L, Hao YM, Dong WJ, Liu Y, Song SM, Shuang SM, Dong C, Gong XJ. Ratiometric fluorescent sensors for sequential on-off-on determination of riboflavin, Ag^+ and l-cysteine based on NPCl-doped carbon quantum dots. Anal Chim Acta. 2021; 1144:1.

[10] Zhu JL, Zhang YH, Chen YH, Sun TM, Tang YF, Huang Y, Yang QQ, Ma DY, Wang YP, Wang M. A Schiff base fluorescence probe for highly selective turn-on recognition of Zn^{2+}. Tetrahedron Lett. 2017; 58(4):365.

 doi:10.20944/preprints202108.0069.v1

[11] Zhang YH, Zhou K, Qiu Y, Xia L, Xia ZN, Zhang KL, Fu QF. Strongly emissive formamide-derived N-doped carbon dots embedded Eu (III)-based metal-organic frameworks as a ratiometric fluorescent probe for ultrasensitive and visual quantitative detection of Ag. Sensor Actuat B-Chem. 2021; 339:129922.
[12] Tu YJ, Wang SP, Yuan XT, Song PF, Wei YL, Qin KH, Zhang Q, Ji XL. Hydrothermal synthesis of Auricularia auricula derived nitrogen, phosphorus-doped carbon dots and application in Ag (I) and 4-nitrophenol detection and bioimaging. Anal Methods. 2020; 12(17): 2237.
[13] Zhu GH, Huang Y, Wang C, Lu LX, Sun TM, Wang M, Tang YF, Shan DD, Wen SJ, Zhu JL. A novel coumarin-based fluorescence chemosensor for Al^{3+} and its application in cell imaging. Spectrochim Acta A. 2019; 210:105.
[14] Zhu JL, Zhang YH, Wang L, Sun TM, Wang M, Wang YP, Ma DY, Yang QQ, Tang YF. A simple turn-on Schiff base fluorescence sensor for aluminum ion. Tetrahedron Lett. 2016; 57(4):3535.
[15] Wu HF, Tong CL. Ratiometric fluorometric determination of silver(I) by using blue-emitting silicon- and nitrogen-doped carbon quantum dots and red-emitting N-acetyl-L-cysteine-capped CdTe quantum dots. Microchim Acta. 2019; 186:723.
[16] Sun Y, Zhang Y, Wang Y, Xia LX. Surface plasmon–catalyzed oxidation of 4-aminodiphenyl disulfide for determination of Ag^{+} ion in aqueous samples. Microchim Acta. 2020; 187:462.
[17] Tang YF, Huang Y, Chen YH, Lu LX, Wang C, Sun TM, Wang M, Zhu GH, Yang Y, Zhang L, Zhu JL. A coumarin derivative as a "turn-on" fluorescence probe toward Cd^{2+} in live cells. Spectrochim Acta A. 2019; 218:359.
[18] Lv CL, Yang CH, Liu LY, Cai Y, Zhang ZC. Organoimido functionalized trinuclear gold(I) clusters with fluorescent chromophore. Rare Met. 2021; 40(6):1437.
[19] Jiang YL, Wang ZY, Dai ZH. Preparation of silicon–carbon-based dots@dopamine and its application in intracellular Ag^{+} detection and cell Imaging. ACS Appl Mater Interfaces. 2016; 8(6):3644.
[20] Zhao Q, Tao GH, Ge CW, Cai Y, Qiao QC, Jia XP. Ultrasensitive fluorescent probe for copper ion based on cadmium selenide/cadmium sulfide quantum dots capped with dimercaprol. Spectrosc Lett. 2018; 51(5):216.
[21] Yang B, Sun NN. A reliable amplified fluorescence-enhanced chemosensor (Eu-MIL-61) for the directional detection of Ag^{+} in an aqueous solution. Dalton Trans. 2017; 46(3):875.
[22] Zhu JL, Lu LX, Wang M, Sun TM, Huang Y, Wang CX, Bao WY, Wang MM, Zou FX, Tang YF. Fluorescence “On-Off” chemical sensor for ultrasensitive detection of Al^{3+} in live cell. Tetrahedron Lett. 2020; 61(21):151893.
[23] Zhang YM, Chen YC, Bai Y, Xue XL, He WJ, Guo ZJ. FRET-based fluorescent ratiometric probes for the rapid detection of endogenous hydrogen sulphide in living cells. Analyst. 2020; 145(12):4233.
[24] Ghirardello M, Ramos-Soriano J, Galan MC. Carbon dots as an emergent class of antimicrobial agents. Nanomaterials. 2021; 11(8):1877.
[25] Gao XX, Zhou X, Ma YF, Qian T, Wang CP, Chu FX. Facile and cost-effective preparation of carbon quantum dots for Fe^{3+} ion and ascorbic acid detection in living cells based on the “on-off-on” fluorescence principle. Appl Surf Sci. 2019; 469:911.
[26] Lee H, Su YC, Tang HH, Lee YS, Lee JY, Hu CC, Chiu TC. One-pot hydrothermal synthesis of carbon dots as fluorescent probes for the determination of mercuric and hypochlorite ions. Nanomaterials. 2021; 11(7):1831.
[27] Zhou X, Gao XX, Song FY, Wang CP, Chu FX, Wu SS. A sensing approach for dopamine determination by boronic acid-functionalized molecularly imprinted graphene quantum dots composite. Appl Surf Sci. 2017; 423:810.
[28] Zhang YM, Chen YC, Fang HB, Shi XC, Yuan H, Bai Y, He WJ, Guo ZJ. A ratiometric fluorescent probe for imaging enzyme dependent hydrogen sulfide variation in the mitochondria and in living mice. Analyst. 2020; 145(15):5123.
[29] Shang YF, Wang HL, Bai H. A coumarin-based turn-on chemosensor for selective detection of Zn(II) and application in live cell imaging. Spectrochim Acta A. 2020; 228:117746.

[30] Wang MM, Wang C, Wang M, Sun TM, Huang Y, Tang YF, Ju JF, Shen LJ, Hu YY, Zhu JL. A dual-functional "on-off-on" relay fluorescent probe for the highly sensitive detection of copper(II) and phosphate ions. ChemistrySelect. 2020; 5(4):1331.
[31] Xu LY, Mo RX, Qi CY, Ren Z, Jia XZ, Kan ZG, Li CL, Wang F. Dual-property blue and red emission carbon dots for Fe(III) ions detection and cellular imaging. Rare Met. 2021; 40(7):1957.
[32] Jorns M, Pappas D. A review of fluorescent carbon dots, their synthesis, physical and chemical characteristics, and applications. Nanomaterials. 2021; 11(6):1448.
[33] Bressi V, Ferlazzo A, Iannazzo D, Espro C. Graphene quantum dots by eco-Friendly green synthesis for electrochemical sensing: recent advances and future perspectives. Nanomaterials. 2021; 11(5):1120.
[34] Bhunia SK, Dolai S, Sun HC, Jelinek R. “On/off/on” hydrogen-peroxide sensor with hemoglobin-functionalized carbon dots. Sensor Actuat B-Chem. 2018; 270: 223.
[35] Li Q, Bai ZL, Xi XJ, Guo ZW, Liu C, Liu XR, Zhao XY, Li ZY, Cheng Y, Wei Y. Rapid microwave-assisted green synthesis of guanine-derived carbon dots for highly selective detection of Ag^{+} in aqueous solution. Spectrochim Acta A. 2021; 248:119208.
[36] Qin X, Yuan CL, Shi R, Wang YL. A double signal optical probe composed of carbon quantumdots and Au@Ag nanoparticles grown in situ for the high sensitivity detection of ellagic acid. J Mol Liq. 2021; 323:114594.
[37] Lu HZ, Li CC, Wang HH, Wang XM, Xu SF. Biomass-derived sulfur, nitrogen co-doped carbon dots for colorimetric and fluorescent dual mode detection of silver (I) and cell imaging. ACS Omega. 2019; 4:21500.
[38] Ma ZM, Liu C, Niu N, Chen ZJ, Li SJ, Liu SX, Li J. Seeking brightness from nature: J-aggregation-induced emission in cellulolytic enzyme lignin nanoparticles. ACS Sustainable Chem Eng. 2018; 6(3):3169.
[39] Huang S, Yang EL, Yao JD, Liu Y, Xiao Q. Red emission nitrogen, boron, sulfur co-doped carbon dots for “on-off-on” fluorescent mode detection of Ag+ ions and l-cysteine in complex biological fluids and living cells. Anal Chim Acta. 2018; 1035:192.
[40] Zhu X, Wang JY, Zhu YH, Jiang HH, Tian D, Xu ZQ, Mei T, Li JH, Xu LJ, Wang XB. Green emitting N,S-co-doped carbon dots for sensitive fluorometric determination of Fe(III) and Ag(I) ions, and as a solvatochromic probe. Microchim Acta. 2018; 185:510.